Heterodyne coherent anti-Stokes Raman scattering (CARS) imaging

Eric O. Potma,* **Conor L. Evans, and X. Sunney Xie**

Department of Chemistry and Chemical Biology, Harvard University, 12 Oxford Street, Cambridge, Massachusetts 02138

We have achieved rapid nonlinear vibrational imaging free of nonresonant background with heterodyne coherent anti-Stokes Raman scattering (CARS) interferometric microscopy. This technique completely separates the real and imaginary responses of nonlinear susceptibility $\chi^{(3)}$ and yields a signal that is linear in the concentration of vibrational modes. We show that heterodyne CARS microscopy permits the detection of weak vibrational resonances that are otherwise overshadowed by the strong interference of the nonresonant background. © 2006 Optical Society of America

OCIS codes: 180.6900, 190.5650.

Coherent anti-Stokes Raman scattering (CARS) microscopy is a nonlinear imaging technique that offers chemical selectivity through vibrational sensitivity.[1] Recent developments in ultrafast light sources and improved detection schemes have advanced CARS microscopy as a useful imaging tool for cellular biology. For example, CARS microscopy has been successfully used to visualize the growth and trafficking of lipid droplets in living cells by utilizing the CH_2 vibrational mode.[2] This study was facilitated by the strong Raman response and the high density of CH_2 groups in lipids, which yielded bright CARS signals. Imaging weaker molecular Raman modes or detecting molecules at lower concentrations (less than $1-10 \times 10^6$ modes per focal volume) with CARS microscopy, however, remains a challenge.

One of the major complications in CARS microscopy comes from the fact that the CARS signal is not background free. The total CARS signal originates from the third-order nonlinear susceptibility of the material, which is a sum of a resonant $\chi_R^{(3)}$ and a nonresonant electronic contribution $\chi_{NR}^{(3)}$. In biological samples, the aqueous environment gives rise to a substantial nonresonant response, which can overwhelm weak resonant signals and significantly reduce imaging contrast. Improving the vibrational contrast in CARS imaging requires suppression of the nonresonant background while the resonant vibrational signal is retained. Although the use of pulses in the picosecond range significantly optimizes the signal-to-background ratio,[3] additional background suppression is needed for observing weak signals. Polarization-sensitive detection[4] and time-resolved CARS[5] have also been used for background rejection, but these techniques also attenuate the resonant contribution and are therefore less suitable for the detection of weak signals.

Interferometric CARS offers the possibility of detecting background-free CARS signals without attenuation. In this approach, the CARS field $E_{as} \propto E_{EX}[\chi_R^{(3)} + \chi_{NR}^{(3)}]$, where $E_{EX} = E_p^2 E_s$ is the effective excitation field, is mixed with a well-controlled reference field E_{LO}, the so-called local oscillator field. The total CARS signal can then be written as

$$S = |E_{LO}|^2 + |E_{as}|^2 + 2E_{LO}E_{EX}\{[\chi_{NR}^{(3)} + \mathrm{Re}\ \chi_R^{(3)}]\cos \Phi + [\mathrm{Im}\ \chi_R^{(3)}]\sin \Phi\}, \tag{1}$$

where Φ is the phase difference between the CARS field and the local oscillator. The last two terms in Eq. (1) are the interferometric mixing terms. An important consequence of Eq. (1) is that the real and the imaginary contributions to the signal now exhibit different dependencies on Φ. If Φ is set to 90°, the resonant imaginary contributions are maximized, while the mixing term containing the nonresonant response vanishes. Similarly, if $\Phi = 0°$, the real part of the signal is uniquely selected. Hence, with proper suppression of the homodyne terms, the real or imaginary response of $\chi^{(3)}$ can be selectively probed in a heterodyne fashion.

As only vibrationally resonant signals give rise to imaginary signal components, heterodyne probing of $\mathrm{Im}\ \chi_R^{(3)}$ allows background-free detection. In addition, the detected signal is linear in the concentration of vibrational modes, which allows for direct concentration measurements. Furthermore, instead of attenuation, interferometric CARS enables linear amplification by increasing the amplitude of the local oscillator. More important, detecting $\mathrm{Im}\ \chi_R^{(3)}$ permits a direct comparison with spontaneous Raman cross sections, facilitating rapid imaging with Raman contrast by means of CARS microscopy.[6] Interferometric detection schemes were previously employed in a microscope configuration for recording CARS spectra free of nonresonant background.[7] These approaches, however, were based on broadband pulses and relatively long integration times and are therefore not optimized for rapid point-by-point imaging. In this Letter we demonstrate heterodyne interferometric CARS microscopy with narrowband picosecond pulses, which permits rapid vibrational imaging with contrast based purely on $\mathrm{Im}\ \chi_R^{(3)}$.

A schematic of our interferometer design is shown in Fig. 1. The Stokes beam at 1064 nm is derived from a 10 ps mode-locked Nd:vanadate laser (PicoTrain, High-Q Lasers), while the tunable 5 ps pump beam is obtained from an intracavity doubled
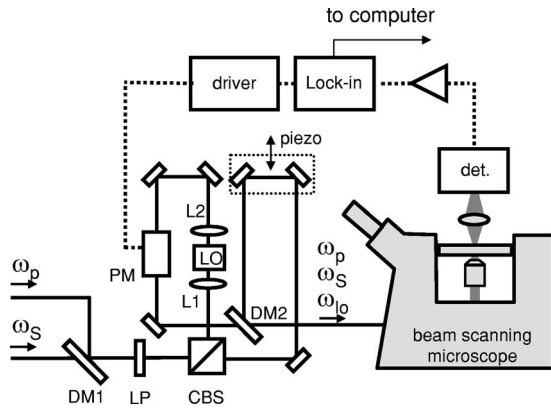
Fig. 1. Schematic of the heterodyne CARS imaging microscope. The output of a Mach–Zehnder interferometer is coupled to a commercial laser scanning microscope (Olympus FV 300). DM1, DM2, dichroic mirrors; LP, long wave pass filter; CBS, cubic beam splitter; L1, L2, objective lenses (0.66 NA, Leica Achro 40×); LO, local oscillator material (d-DMSO); PM, phase modulator (New Focus 4003); det, photomultiplier tube (Hamamatsu R3896).

optical parametric oscillator (Levante, APE Berlin) that is synchronously pumped by the Nd:vanadate source. The pump and Stokes beams are collinearly combined and sent into a Mach–Zehnder-type interferometer. One of the arms contains a cell of deuterated dimethyl sulfoxide (d-DMSO) for generating a strong nonresonant signal at the anti-Stokes frequency that serves as the local oscillator. A phase modulator applies an $\sim 10°$ phase modulation at 10 MHz to the local oscillator beam. The other arm of the interferometer includes a piezo-controlled stage for accurately adjusting the path-length difference between the arms.

The local oscillator beam is collinearly overlapped with the pump and Stokes beams on a dichroic mirror and directed to a commercial beam-scanning microscope. A 1.15 NA water immersion objective lens focuses the beams into the sample. Power levels at the sample are $10-30$ mW for the pump–Stokes beams and $1-100$ nW for the local oscillator beam, as measured with a photodiode. At the sample, the generated CARS field is directly mixed with the copropagating local oscillator field. The 10 MHz phase modulation now becomes an amplitude modulation on the signal through the (heterodyne) mixing terms in Eq. (1). The signal is measured with a photomultiplier and fed into a lock-in amplifier for isolating the heterodyne signal.

We have chosen the copropagating configuration of the local oscillator because it leaves the overlap of the CARS and local oscillator beams unchanged while the beams are rapidly scanned in the microscope. We obtain complete constructive or destructive interference of the CARS field with the local oscillator field, indicating that the phase fronts of the mixing fields in the focal volume are maintained well by the interferometer. Figure 2 (top) shows the measured heterodyne signal as a function of the local oscillator amplitude. As expected, a linear amplification of the signal is observed with amplifications of as much as 50 times. It is important to point out that this amplifi-

cation is achieved without increasing the intensity of the incident pump and Stokes beams but by varying the low-power local oscillator strength instead. The dependence of the heterodyne CARS signal on dodecane concentration is shown in Fig. 2 (bottom). With the Raman shift tuned to the 2845 cm^{-1} CH$_2$ vibrational resonance of a dodecane solution, a linear dependence is seen on dilution with nonresonant deuterated dodecane. In our fast scanning microscope, a concentration of $\sim 1\%$ dodecane is accurately detected with a pixel integration time of 10 μs. Higher sensitivity can be obtained by increasing the integration time.

Figure 3 demonstrates the capability of heterodyne CARS to selectively image the imaginary and real parts of a material's nonlinear susceptibility. The noninterferometric CARS image of a NIH3T3 cell taken at 2845 cm^{-1}, the CH$_2$ symmetric stretching vibration of lipids, is shown in Fig. 3(a). A strong nonresonant background is present, which gives rise to an offset and mixes with the vibrational signal in a heterogeneous manner. Figures 3(b) and 3(c) show the disentangled imaginary and real responses of the sample. In the Im $\chi_R^{(3)}$ image, the background is absent, and contrast arises solely from the CH$_2$ vibrational mode. The imaginary response was maximized by adjusting the nonresonant signal from the aqueous background to zero ($\Phi = 90°$). The real response was found by maximizing the nonresonant signal ($\Phi = 0°$). In addition to the real response of the vibrational mode, the background is prominent in the Re $\chi^{(3)}$ image, limiting the vibrational contrast. It should be noted that the Im $\chi_R^{(3)}$ image is essentially a Raman image, taken at a rate 3 orders of magnitude
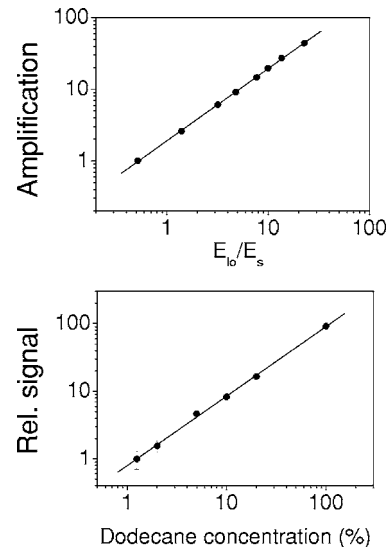

Fig. 2. Dependence of the heterodyne signal on the local oscillator's amplitude and scatterer concentration. Top, amplification of the heterodyne CARS signal from a glass coverslip as a function of the local oscillator's strength (filled circles). Amplification is defined as the ratio of the heterodyne CARS signal to the noninterferometric CARS signal. Solid line, linear fit to slope 1.0. Bottom, heterodyne CARS signal as a function of the concentration of dodecane in deuterated dodecane. The signal was measured at 2845 cm^{-1} (filled circles). Solid line, linear fit to slope 1.02.
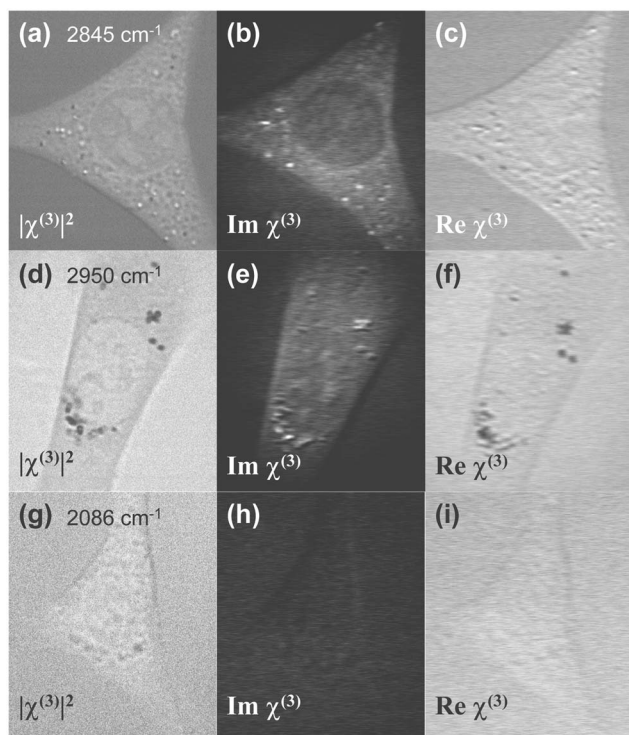
Fig. 3.   Comparison of heterodyne CARS with noninterferometric CARS imaging of live NIH 3T3 cells. The noninterferometric image of the cell in (a) was taken at the peak of the symmetric CH_2 vibration (2845 cm^{-1}); the measured imaginary and real responses are given in (b) and (c), respectively. The noninterferometric image of the cell in (d) was taken on the blue side of the CH-stretching band at 2950 cm^{-1}; the isolated imaginary and real responses are shown in (e) and (f), respectively. (g), (h), (i) Noninterferometric and imaginary and real response images, respectively, off resonance at 2086 cm^{-1}. Image dimensions are 35 μm $\times$ 40 μm.

faster than current spontaneous Raman scattering microscopes can offer.

At 2950 cm^{-1}, the noninterferometric CARS image in Fig. 3(d) shows negative contrast. This is a direct result of the spectrally dispersive nature of the real response, which leads to destructive interference with the nonresonant background at the blue side of the vibrational resonance [Fig. 3(f)]. The imaginary response in Fig. 3(e) displays positive contrast instead, and it is unaffected by background mixing. As a result, weak vibrational signals that are overwhelmed by background interference effects in regular CARS can now be observed. The contrast in the Im $\chi_R^{(3)}$ image is attributed to the previously unseen CH_3 vibration of proteins. Figures 3(g)–3(i) demonstrate that tuning off-resonance to 2086 cm^{-1} causes the imaginary response to virtually disappear [Fig. 3(h)], clearly demonstrating that this heterodyne method detects primarily vibrational resonances and that intrinsic phase differences due to sample dispersion are only a minimal contribution.

In the images shown, the shortest lock-in integration time was 10 μs, whereas the longest available pixel dwell time was 8 μs. This difference results in a loss of resolution along the fast scanning axis by a factor of $\sim$2, which can be easily corrected by optimizing the apparatus. When the beam is scanned, a position-dependent phase difference between the CARS field and the local oscillator is introduced by the dispersive properties of the (high-N.A.) microscope optics. However, we found this effect to be very small: In the current configuration, the position-dependent phase difference is less than 10° over a 50 μm $\times$ 50 μm scanned area at a Raman shift of 2845 cm^{-1}. This small phase variation gives rise to the slight gradient in the background of Figs. 3(b) and 3(e). Note that this phase shift decreases for smaller Raman shifts.

In summary, heterodyne CARS microscopy permits separate visualization of the real and imaginary responses of samples at relatively fast imaging speeds. The imaginary response is free from nonresonant background, is linear in the concentration of vibrational modes, and can be directly correlated with spontaneous Raman scattering. Moreover, we have shown that heterodyne CARS imaging is useful for amplifying weak signals. We expect that, with the current improvements, the weak responses observed from certain biologically relevant molecular compounds will yield higher-contrast CARS images.

*Present address, Department of Chemistry, University of California at Irvine, Irvine, California 92697.

References

1. J. X. Cheng and X. S. Xie, J. Phys. Chem. B **108**, 827 (2004).
2. X. L. Nan, J. X. Cheng, and X. S. Xie, J. Lipid Res. **44**, 2202 (2003).
3. J. X. Cheng, A. Volkmer, L. D. Book, and X. S. Xie, J. Phys. Chem. B **105**, 1277 (2001).
4. J. X. Cheng, L. D. Book, and X. S. Xie, Opt. Lett. **26**, 1341 (2001).
5. A. Volkmer, L. D. Book, and X. S. Xie, Appl. Phys. Lett. **80**, 1505 (2002).
6. R. W. Hellwarth, in *Progress in Quantum Electronics*, J. H. Sanders and S. Stenholm, eds. (Pergamon, 1977), pp. 1–68.
7. C. L. Evans, E. O. Potma, and X. S. Xie, Opt. Lett. **29**, 2923 (2004).